Increased precipitation in NW Europe triggered by the Hudson Bay Ice Saddle collapse

Claire Ansberque[1,2*], Frederik Schenk[1,2,3], Chris Mark[4,6], Petter Hällberg[2,5], Malin E. Kylander[1,2], Frank McDermott[6], Alessandro Maltese[4]

[1] Department of Geological Sciences, Stockholm University, Sweden. [2] Bolin Centre for Climate Research, Stockholm University, Sweden. [3] Department of Geosciences and Geography, University of Helsinki, Finland. [4] Department of Geology, Swedish Museum of Natural History. [5] Department of Earth Sciences, Uppsala University, Sweden. [6] School of Earth Sciences, University College Dublin, Ireland.

*Corresponding author: claire.ansberque@geo.su.se

Abstract

The collapse of the Hudson Bay Ice Saddle (HBIS), whose freshwater signal is dated between 8.6 and 8.5 ka b2k, is increasingly viewed as the primary driver of the abrupt '8.2 ka' cooling anomaly. Yet linking the two implies that the climatic repercussion of the HBIS collapse lagged by centuries – a delay at odds with some climate models projecting that meltwater forcing can influence climate change within just a few decades. Here, we present a stalagmite-based geochemical record spanning 11.1–7.5 ka from western Ireland – a region highly sensitive to the North Atlantic climate – that provides direct evidence that the HBIS collapse triggered a rapid hydroclimatic change in the region. Based on the stalagmite $\delta^{18}O$, mirroring North Atlantic seawater $\delta^{18}O$, and its Sr/Ca data, we document a pronounced increase in precipitation coinciding with the HBIS collapse and a slowdown of the AMOC at 8.6 ka. This precipitation trend persists throughout the '8.2 ka' event and does not return to the level pre-HBIS collapse until 7.9 ka, suggesting a slow recovery of the hydroclimate, independent of temperature direction. Our findings outline what may lie ahead for NW Europe in the coming decades if meltwater flux keeps accelerating and the AMOC weakens.

Introduction

Several climate models show that freshwater discharge from a melting ice sheet can weaken the Atlantic Meridional Overturning Circulation (AMOC)[1,2], thereby generating widespread climatic anomalies[3,4,5]. However, the timescales linking freshwater input to climatic response remains uncertain[6,7]. To improve our capability to predict the climatic repercussion of potential freshwater forcing in the context of current rapid Arctic ice loss and potential AMOC decline[8,9], a better understanding of the time lag between the two is required.

A large meltwater discharge occurred between 8.6 and 8.5 ka before the year 2000 (b2k; the reference timescale used throughout), when benthic foraminifera $\delta^{18}O$ from the Labrador Shelf captured a pronounced freshening, attributed to the collapse of the Hudson Bay Ice Saddle (HBIS)[10]. With an estimated freshwater reservoir of 451,000 km^3 [10] and a potential 100-year forcing strength of up to 0.6 Sv[11], the HBIS collapse represents one of the largest meltwater releases of the Holocene, and has recently been identified as the primary driver of the '8.2 ka' cooling event[11,12] – one of the sharpest climatic anomalies of the Holocene[13,14,15]. However, the timing of the '8.2 ka' event complicates this interpretation. Ice cores[13,15,16] and speleothems[17] from the northern hemisphere place the cooling between 8.3 and 8.0 ka[17], implying at least a 200-year lag between the HBIS collapse and its imputed climatic impact. Such a delay contrasts with several climate model simulations, which show that meltwater forcing can slow the AMOC and change the climate within only a few decades[7,18,19]. This discrepancy has led to competing hypotheses: either the '8.2 ka' event lagged centuries behind the HBIS collapse[11], or it reflects the compounded effect of multiple freshwater pulses facilitated by the loss of the saddle, including the Lake Agassiz–Ojibway outburst[20,21], which was first thought as the main driver of the '8.2 ka' anomaly[22].

Coinciding with the freshwater signal of the HBIS collapse, two key components of the AMOC – the North Atlantic Current (NAC)[23], which forms its upper limb, and the Iceland–Scotland Overflow Water (ISOW)[24], a major part of its lower limb – show signs of freshening and weakening, respectively, at 8.6 ka (Figs 1 and 2b, c, d). While these data were not linked with the HBIS collapse at the time of their publication, the recent evaluation of the saddle collapse as a major freshwater influx suggests that it could have been the dominant forcing[11,12]. Together, these observations raise the question: was the HBIS collapse already influencing the climate centuries before the '8.2 ka' event by slowing down the AMOC?

Recent climate model simulations indicate that a weakened AMOC would strengthen the North Atlantic winter storm track, thereby increasing precipitation in parts of northern Europe[5], particularly over the Irish–British Isles

and Denmark[4]. Several regional hydroclimate archives show signals consistent with this simulated response at the time of the HBIS collapse at these localities. At Højby Sø in Denmark, lake-productivity data reveal a shift toward wetter and windier conditions beginning at 8.6–8.5 ka, persisting until the '8.2 ka' event[25]. Storm-deposit records from nearby Filsø lake similarly document enhanced storminess and precipitation at 8.5–8.4 ka[26]. Although these changes coincide with the HBIS freshwater pulse, they have not been directly linked to it. Demonstrating such a connection requires archives that can capture both the oceanic and atmospheric fingerprint of meltwater discharge with high chronological resolution. Speleothems have proven valuable in doing so[27,28]. Their amenability to precise radiometric dating and capacity to provide high-resolution climatic information[29,30] can help assess the time lag between a large meltwater discharge and its climatic fallout.

Here we present a hydroclimate record spanning from 11.1 to 7.5 ka, derived from a fast-growing stalagmite from Cliff Cave, western Ireland. This site is ideally situated to capture the climatic impacts of freshwater forcing on the AMOC due to its immediate proximity to the North Atlantic (Fig. 1). The chronology of this early Holocene stalagmite is constrained by fourteen U-Th dates, and climatic impacts are inferred from stable isotope ($\delta^{18}O$, $\delta^{13}C$) and Sr/Ca ratio. We show a clear link between the Cliff Cave stalagmite $\delta^{18}O$ with that of the eastern North Atlantic waters, and between hydroclimate-sensitive proxies in the stalagmite and the HBIS collapse (Fig. 2).

Site description

Cliff Cave is located on the west coast of Ireland, in County Clare (53.068°N, 9.359°W), where it is hosted in the early Carboniferous Burren Limestone Formation (Figs. 1 and SD1). Its entrance lies 9.5 m below current sea level and the cave is 3.5 km in length[31]. Currently, due to relative sea-level rise since the early Holocene[32], the cave is partly submerged and accessible only during calm sea conditions to experienced open-water divers. Because of its hazardous access, the cave is currently unmonitored and only the first kilometre has been properly surveyed. The stalagmite analysed in this study (Cliff Cave stalagmite) was opportunistically collected about 700 m from the cave's entrance and was submerged 6 m below the present-day low water mark[31]. The ground surface above the cave consists of bare rock, characteristic of the Burren area, with the nearest agricultural lands situated ~2 km southwest of the cave (Fig. SD1). The earliest evidence of sustained human occupation in the region is dated to 6.9-5.6 ka[33]. Land use change from anthropogenic activities at the cave surface is therefore considered to have had a limited impact on the stalagmite deposition and chemistry during its growth. Diefendorf et al.[34] measured $\delta^{13}C$ values for the Burren Limestone ranging from 3.2 to 3.6

‰ at sites between 10 and 40 km from Cliff Cave. Local sea level reconstructions place sea level at ~38 m bsl at 11.1 ka, increasing to ~10.5 m bsl by 7.5 ka[32]. We note that sea level estimate at 7.5 ka is consistent with the fact that Cliff Cave stalagmite stopped growing around that time, suggesting a possible submersion of the cave not long after.

Ireland has a maritime climate, with a mean annual air temperature (MAAT) of 10 °C (Met Éireann). Precipitation records from 2005-2024, from Lisdoonvarna meteorological station (~10 km southeast of Cliff Cave) indicate that the area experiences the lowest rainfall amount in spring (April to June; ~86 mm) and the highest amount in fall (October to December; ~173 mm; Supplementary Table).

Results and Discussion

Cliff Cave stalagmite $\delta^{18}O$ detects freshening of the eastern North Atlantic at 8.6 ka

The $\delta^{18}O$ signal of Cliff Cave stalagmite ($\delta^{18}O_{Cliff}$) is relatively stable from c. 11.0 to 8.6 ka, albeit with a slight (0.3 ‰) decline to an average value of -3.6 ‰ between c. 9.5 and 8.6 ka (Fig. 2a). At 8.6 ka, $\delta^{18}O_{Cliff}$ exhibits a clear decrease and remains relatively low throughout, with an average value of -4.3 ‰. This millennial trend closely mirrors $\Delta\delta^{18}O$ foraminifera and sub-thermocline salinity records from marine sediment core RAPiD-12-1K[23], which records the NAC dynamics (Fig. 2b, c), and bottom current velocity data from MD99-2251[24], a proxy of the ISOW strength (Fig. 2d). The fact that $\delta^{18}O_{Cliff}$ parallels these marine proxies strongly suggests that, in the early Holocene and on a millennial timescale, Cliff Cave drip water is derived from precipitation sourced predominantly from the eastern North Atlantic surface water, and that the isotopic signature of this precipitation ($\delta^{18}O_p$) is closely linked to the surface seawater ($\delta^{18}O_{sw}$) with minimal temporal variability in isotopic fractionation effects from source to sink.

The onset of the gradual decline in both RAPiD-12-1K and MD99-2251 datasets at 8.6 ka coincides with the freshwater signal of the HBIS collapse and with a first drop in *N. Pachyderma* sinistral (Fig. 2f, h). These observations are consistent with a progressive freshening of the North Atlantic due to meltwater discharge[23,24] initiated by the HBIS collapse at 8.6 ka[10]. The correlation between $\delta^{18}O_{Cliff}$ and these marine records therefore suggests that the HBIS freshwater pulse reduced the North Atlantic $\delta^{18}O_{sw}$, and that this change was transferred to $\delta^{18}O_{Cliff}$ drip water through rapid ocean-atmosphere teleconnection. Further, Cliff Cave $\delta^{18}O$ displays a large negative excursion (made of five data points) centred at 8.4 ka. This negative excursion coincides with a second substantial drop in *N. Pachyderma* sinistral and a short-lived $\delta^{18}O$ negative excursion in Kaite Cave stalagmite[35] (Fig. 2h, i), which were both attributed to a drainage episode of Lake Agassiz-

Ojibway[24,35]. Taken all together, the data suggest that at 8.6 ka the HBIS induced sufficient changes in North Atlantic $\delta^{18}O_{sw}$ to appear as a progressive decline in $\delta^{18}O_{Cliff}$ with almost no time lag between the two. The following freshwater discharge from Lake Agassiz–Ojibway then produced a distinct negative $\delta^{18}O_{Cliff}$ excursion at 8.4 ka, likely reflecting the compounded impact of both meltwater discharges on the North Atlantic water chemistry.

During the '8.2 ka' event (as defined by the wide blue band on Fig. 2), the $\delta^{18}O_{Cliff}$ signal bounces back to slightly heavier values (above -4 ‰; Fig. 2a; the negative excursion ~8.1 ka is represented by two data points and is not discussed further). This slight rebound contrasts with other speleothem $\delta^{18}O$ records from western Europe, in which the '8.2 ka' event is characterised by a centennial-long period of lighter $\delta^{18}O$ values[17,35] (Fig. 2i). However, the rebound in $\delta^{18}O_{Cliff}$ during the '8.2 ka' event correlates with one in $\Delta\delta^{18}O$ foraminifera and sub-thermocline salinity records of RAPiD-12-1K[23] (Fig. 2a, b, c). This covariation further supports the connectivity between the $\delta^{18}O_{Cliff}$ signal and the North Atlantic $\delta^{18}O_{sw}$ and the idea of a rapid ocean-atmosphere teleconnection. In addition, it is possible that the slight rebound in $\delta^{18}O_{Cliff}$ reflects a cave-cooling effect superimposed on the oceanic source signal, since lower cave temperatures enhance the calcite–water fractionation factor during drip-water precipitation, which could have raised $\delta^{18}O_{Cliff}$ during the '8.2 ka' cooling event. Assuming a ~0.2 ‰ $°C^{-1}$ [36] and a $\delta^{18}O_{Cliff}$ rebound of ~0.7‰ (Fig. 2a), the cave might have cooled by ~3.5°C during the '8.2 ka' event.

Cliff Cave stalagmite Sr/Ca records increased precipitation at 8.6 ka

Coinciding with the decline in $\delta^{18}O_{Cliff}$ at 8.6 ka, Cliff Cave stalagmite Sr/Ca (Sr/Ca_{Cliff}) reaches a tipping point and begins a pronounced, sustained decrease, with no return to higher values until 8.4 ka (Fig. 2e, note the reverse y-axis scale). Here we associate this decrease to wetter conditions (Methods). A recent inter-model comparison by Vacca et al.[37] showed that a strong weakening of the AMOC leads to a more frequent occurrence of the North Atlantic Oscillation positive (NAO+) phase. During NAO+ phases, the North Atlantic winter storm track is typically positioned over northern latitudes, where intensified westerly winds and a strengthened jet stream steer storm systems toward northern Europe, resulting in wetter and stormier winters in the Irish-British Isles. Here, we propose that the increased precipitation trend observed from 8.6 to 8.4 ka in Cliff Cave stalagmite is linked to the development of NAO+ conditions favoured by the slowdown of the AMOC, initiated by the HBIS freshwater pulse. Smith et al.[38] showed that speleothems from Cueva de Asiul, Spain, ceased to grow at 8.6 ka due to drier and colder conditions. They attributed this observation to a predominance of NAO+ conditions, which aligns well with our findings since an NAO+ phase produces a see-saw climate

patterns between Spain and Ireland's latitudes: drier and colder winters in Spain associated with wetter and milder winters in Ireland.

We also note that an increase in precipitation at 8.6 ka could imply a precipitation amount effect on $\delta^{18}O_{Cliff}$, which would lower the ratio as seen on Fig. 2a at that time. However, modern $\delta^{18}O_p$ measured at the Valentia Observatory on the west coast of Ireland, is only weakly to moderately correlated to precipitation amount on decadal timescales[39], suggesting that its effect is unlikely to be the primary control of the $\delta^{18}O_{Cliff}$ variation at 8.6 ka.

Between 8.8 and 8.6 ka, the Sr/Ca_{Cliff} displays high fluctuating values, seemingly interrupting a millennial-long increase trend (Fig. 2e; Methods). It is interesting to note that this period coincides with a sub-surface warming of the Labrador Shelf waters prior to the HBIS collapse[10] (Fig. 2g), although the shortness of this period does not permit a clear connection to be established. After 8.4 ka, Sr/Ca_{Cliff} increases again reaching maximum values (0.009) around 7.8 ka (Fig. 2e). This short period correlates with a recovery of the ISOW strength, which was interpreted as an AMOC overshoot[24] (Fig. 2d). The limited data between 7.9 ka and the end of our record makes it difficult to assess the correlation between this AMOC recovery and the renewed high Sr/Ca_{Cliff} values, but the covariation between the two further supports the argument that the region's hydroclimate is tightly coupled to the state of the ocean overturning circulation in the adjacent North Atlantic Ocean.

During the '8.2 ka' event, the Sr/Ca ratio of Cliff Cave stalagmite increases again, but remains lower than prior to the 8.6 ka HBIS collapse (Fig. 2e). This indicates that overall wetter conditions prevailed throughout the '8.2 ka' event at the study site. This is supported by the fact that Cliff Cave stalagmite continued growing during the '8.2 ka' event, indicating absence of prolonged freezing conditions at the cave surface. This observation aligns with a precipitation-proxy compilation by Morrill et al.[40], which shows that parts of northern Europe (particularly Scandinavia) experienced enhanced precipitation during the '8.2 ka' event. This suggests that heightened precipitation is a persistent climatic fallout of a weakened AMOC in this region, independent of temperature direction.

In summary, this study presents a high-resolution hydroclimatic record for a key Atlantic margin site from 11.1 to 7.5 ka. The record shows a marked increase in precipitation at 8.6 ka, which when compared to the existing literature[25,26,40], could have extended across NW Europe. We interpret this hydroclimatic shift as evidence for a rapid reorganization of atmospheric circulation linked to a weakened overturning circulation, triggered by the HBIS collapse at 8.6 ka (Fig. 2). On the basis of climate model simulations, a possible mechanism explaining this hydroclimatic shift is the strengthening of the North Atlantic winter storm track[4,5,37]. A persisting unknown

in climate model simulations is the time lag between a weakening AMOC and its climatic fallout; our finding suggests that it could occur over a human life time.

To further contextualise our findings, two one-point-correlation maps produced using the ERA5 dataset (1950–2022)[41] reveals that the near-surface temperatures at the Cliff Cave site are strongly correlated with those across the North Atlantic, particularly across a broad NE-SW band, which closely mirrors the simulated North Atlantic winter storm track[4] (Fig. 3). Although the current trajectory of the AMOC is uncertain[9,42], these maps highlight the direct exposure of NW Europe to climatic extremes should the North Atlantic winter storm track strengthen. Long-term precipitation trends in Ireland from 1910 to 2019 show an increasing contribution of heavy and extreme rainfall to annual totals[43]. While an empirical link between the ongoing weakening of the AMOC and strengthening of the North Atlantic winter storm track has yet to be established, our findings indicate that such a connection is plausible.

Acknowledgments

This work was supported by the Swedish Research Council for Sustainable Development (FORMAS; Research Grant number: 2022-00492; PI: C.A), the Bolin Centre for Climate Research RT3, RT4 seed money (PI: C.A), and the Riksmusei Vänner (C.A and C.M). F.S. is funded by FORMAS (Research Grant numbers 2020-01000 and 2023-01631). C.A thanks Haoyi Yao (IGV, Stockholm University) for performing the IRMS analysis, and Karin Wallner, Per-Olof Persson and Andreas Karlsson (all at the Swedish Museum of Natural History) for analytical assistance. NordSIMS-Vegacenter is funded by the Swedish Research Council as a national research infrastructure (Dnr. 2021-00276). Cave divers Jim Warny and Michal Marek are thanked for retrieving the stalagmite from Cliff Cave.

Methods

All supplementary information associated to this work can be found in the Supplementary Data and Table, and will be deposited to the Bolin Centre for Climate Research Database.

Cliff Cave stalagmite

The Cliff Cave stalagmite is a 42.6-cm-long specimen, with an average radius of 6.7 cm (SD: 0.9 cm; Fig. SD2). For analysis purposes, the stalagmite was cut open along its growth axis, revealing regular, fine laminae, which suggests limited diagenetic alteration. The stalagmite candle shape and its fine lamination suggest relatively constant within-cave climatic conditions over millennial timescales.

A main change in growth direction is observed between 325-320 mm depth (distance from the top of the stalagmite; Fig. SD2). The U-Th ages and the age-depth model calculated with StalAge[44] (see sections below) indicate a relatively continuous growth, with no hiatus detected (Fig. SD3). The fact that the U-Th ages bracketing this change in growth direction are indistinguishable within uncertainties, likely explains the lack of clear hiatus on the age-depth model. This also suggests that if the stalagmite growth was interrupted, it resumed rapidly. The stalagmite growth rate calculated from the age-depth model indicates, however, an anomalously fast growth between 330-318 mm, which does represent the change in growth direction hiatus. The good correlation between the true position of the hiatus and its position on the growth rate profile indicates that the StalAge age-depth model is reliable. Nonetheless, we performed an age-depth model for the top 318 mm of the stalagmite (i.e., above the hiatus), which is, as expected, identical to the first age-depth model from 9.9 to 7.5 ka.

Below 318 mm (between the base of the stalagmite and the above-mentioned change in growth direction), several growth intervals consist of visible millimetric columnar minerals, suggesting short-lived change in drip water flow regime. This type of lamina is only present in this section of the stalagmite (11.1-10.2 ka) and might reflect short-lived hydrographic shifts at the cave's surface (Fig. SD2).

Mineralogy

We examined the dominant mineralogy of Cliff Cave stalagmite in forty Fourier Transform InfraRed – Attenuated Total Reflectance (FTIR-ATR) spectra obtained from 10-mg sample powders collected every 1 cm along the stalagmite length and parallel to the lamina (Supplementary Table). We used a benchtop ThermoFisher Nicolet iS5 FTIR spectrometer equipped with an iD7 diamond ATR crystal. FTIR-ATR is a rapid (3 min per sample), non-destructive and chargeless technique. Each sample spectrum was determined over 100 scans with a 4 cm^{-1} resolution and a data spacing of 2 cm^{-1}. Before sample spectrum acquisition, a background measurement was performed over 32 scans with the same resolution and data spacing, and subsequently subtracted from the sample spectrum to remove any atmospheric compounds present in the laboratory. FTIR-ATR spectra show that calcite is the main mineral and carbonate phase.

A subset of these samples was analysed by XRD analyses (see the Supplementary Table for scan parameters), confirming calcite as the dominant mineral. No aragonite or dolomite were detected. A few samples show the presence of quartz (at the bottom of the stalagmite); XRD spectra indicate quartz represents less than 1% in these samples.

U-Th ages

U-Th ages were acquired in two different laboratories (Supplementary Table). A first set of ages (nb= 2, top and bottom of the stalagmite) was acquired in 2018, at the National Centre for Isotope Geochemistry in the School of Earth Sciences, University College Dublin (Ireland), following a procedure described in Fankhauser et al.[45]. A second set of ages was measured at the NordSIMS-Vegacenter, Swedish Museum of Natural History (NRM, Sweden), following the procedure described below.

U-Th ages were obtained along the main growth axis of Cliff Cave stalagmite and above and below suspected change in growth direction (Fig. SD2). A minimum of 50 mg of sample powder was hand-drilled parallel to the lamina. Powders were dissolved and ion-exchanged to yield separated U and Th aliquots in the clean laboratory of the Department of Geosciences at the NRM, following a standard procedure[45]. A ^{229}Th-^{233}U-^{236}U mixed spike was gravimetrically prepared from a ^{233}U/^{236}U solution prepared at ETH Zurich using the approach of Stirling et al. (2005)[46] and a ^{229}Th solution following Andersson and Schöberg (2012)[47]. The target ^{233}U/^{229}Th atomic ratio was 270, which was confirmed by a thermal ionisation mass spectrometry (TIMS) measurement of 269.3 ± 1 (2SD; see the following section).

Isotope ratios were measured on a Nu Plasma 3 multi-collector inductively coupled plasma mass spectrometer (MC-ICPMS). After dissolution, spiking, and ion-exchange, samples were introduced as mixed U-Th solutions in a 2M HNO_3 matrix doped with HF using a Cetac Aridus 3 desolvating nebuliser, with Ar nebuliser (27-28 PSI) and sweep (4.4-6.8 L/min) gases. Sample consumption per single analysis was ~600-700 µl. A two-line routine with magnet jumps was employed, using the detector assignments shown in Table 1. Each analysis comprised one block of 24 cycles, at 14 s/cycle (5 s/line, 2s magnet settling time). Sample intensity was c. 30 V (^{238}U), and yield was c. 1000 V / ppm by mass. On-mass-zeros were measured using the same routine for 6 cycles in blank acid prior to each analysis. Analyses were preceded by a 45 s transfer time and followed by a 300 s wash in 2M HNO_3 doped with HF.

Table 1: Nu Plasma 3 detector configuration used for U-Th measurements

Detector	H2	H1	Ax	L1	L3	L4	IC0 (Daly)
Preamplifier (Ω)	10^11	10^11	10^11	10^12	10^11	10^11	-
Line 1	238U	m237	236U	235U	233U	232Th	230Th
Line 2				234U			229Th

Baseline-corrected tailings on ^{230}Th and ^{229}Th were measured at masses 237, 236.5, 235.5, and 233.5 using a magnet-jumping multi-line method with ^{238}U in a Faraday cup and other masses in a Daly detector at the IC0 position, and interpolated using a power-law function. Tails were measured at the start and end of each session, and were indistinguishable. Baseline-corrected tailings on ^{235}U, ^{236}U, ^{234}U, ^{233}U, and ^{232}Th were obtained by measurements on masses 237, 236, and 233 during in-run analyses of CRM-112A, and interpolated using a power-law function. After correction for baselines, blanks, and tailings, measured U ratios were internally corrected using the in-house spike ^{236}U/^{233}U (0.957210 ± 0.000054) or certified values (SRM-U500 only, employed as a secondary standard and treated as an unknown during analysis), and finally normalised to CRM-112A ^{238}U/^{234}U, analysed after every four unknowns and interpolated linearly.

Normalised ^{230}Th/^{232}Th ratios were corrected using IRMM-035, run at the end of each session; ^{230}Th/^{238}U ratios were corrected using the in-house ^{229}Th-^{233}U-^{236}U mixed spike described below. Abundance sensitivity on mass 237 was c. 11 ppm. Data were reduced offline using an in-house spreadsheet, and ages were calculated using Isoplot[48]. All ages are corrected for detrital thorium using a fixed initial ^{230}Th/^{232}Th of 0.8 ± 0.4[49] and reported in calendar years before 2000 CE (common era; b2k timescale). Age uncertainties are reported at the 2σ level. The age-depth model was calculated with the StalAge R package[44]; four out of eighteen ages were excluded based on StalAge model.

TIMS analysis

A ^{236}U–^{233}U–^{229}Th spike was prepared by gravimetric mixing using previously characterized ^{236}U–^{233}U double and ^{229}Th single spikes at the Department of Geosciences at the Swedish Museum of Natural History, Stockholm. To calibrate the U/Th ratio of the mixture, about 500 mg of mixed spike were weighed into 3 Teflon vials and doped with a U ICP-standard (Fluka 2022, 1002 ± 15.8 µg/mL) to achieve ^{238}U/^{236}U in the range of 6–15. Another 3 vials were doped with a Th ICP-standard (Aristar 2022, 9.990 ± 0.031 µg/mL) to achieve ^{232}Th/^{229}Th in the range of 7–15. Isotopic equilibration was achieved at 80 °C on a hotplate for 72 h, the spike-sample mixtures dried down, and U and Th separated by ion exchange chromatography using AG 1-X8 (200-400 mesh) with 7 M HNO_3 and 6 M HCl, respectively.

Isotope analyses were carried out on a Thermo Scientific Triton thermal ionization mass spectrometer. Uranium was loaded onto zone-refined Re double filaments in 2 µL 0.3 M HNO_3 and measured in multi-collection mode using 1011 Ω amplifiers and the secondary electron multiplier (SEM) detector for ^{235}U. Corrections for mass fractionation were carried out internally against ^{236}U/^{233}U = 0.95721 of the U double spike. Thorium was loaded onto zone-refined Re single filaments on top of 1 µL 0.25 M H_3PO_4, followed by addition

of 4 µL graphite activator. Measurements were performed via peak jumping on masses 232 and 229 using the SEM detector at temperatures between 1750–1800 °C. Mass fractionation correction was carried out externally against a gravimetrically mixed in house standard-spike solution with $^{232}Th/^{229}Th = 10$, measured at the same temperature interval.

Concentrations were determined using the general framework for isotope dilution[50]. Assuming natural abundances, the standard solution was used in place of the isotopic tracer to derive the abundances of isotopes in the spike. This way, U/Th ratios in the mixed spike are found to be $^{233}U/^{229}Th = 269.3 \pm 1.0$ and $^{236}U/^{229}Th = 257.7 \pm 1.0$ (2SD, n = 9).

Stable isotopic analysis

About 200 µg of sample powder was collected every ~1 mm along the growth axis of Cliff Cave stalagmite using a hand drill mounted with a 0.8 mm drill bit. Samples were placed in exetainer vials and oven-dried overnight at 90°C. After laying the vials horizontally, 100 µL of H_3PO_4 (purity ≥ 99%) was added onto the vial wall without touching the sample powder, and once closed, 100 mL/min of helium was flushed for 10 minutes into the vials through their exetainer. Vials were then put vertically to allow acid/sample reaction and CO_2 production; the reaction took place at room temperature overnight. Oxygen and carbon isotopic ratios were measured on a Thermo Fisher Scientific MAT253 GasBench II mass spectrometer at the Stable Isotope Laboratory, Stockholm University (Supplementary Table). Standard precision was below ± 0.08 ‰. Cliff Cave stalagmite stable isotopes are reported relative to the Vienna Pee Dee Belemnite (VPDB) standard. Data quality control and instrumental drift were checked by employing a sample-standard bracketing approach using four carbonate standards: NBS 18 (-5.014 ‰ $\delta^{13}C$; -23.2 ‰ VPDB $\delta^{18}O$), IAEA-603 (2.46 ‰ $\delta^{13}C$; -2.37 ‰ VPDB $\delta^{18}O$), Carm 2 (2.59 ‰ $\delta^{13}C$; -1.05 ‰ VPDB $\delta^{18}O$) and $CaCO_3$ Merck (-8.76 ‰ $\delta^{13}C$; -18.39 ‰ VPDB $\delta^{18}O$). These were prepared in the same way as the stalagmite sample powders.

$\delta^{18}O_{Cliff}$ ranges from -5.5 ‰ to -2.7 ‰ and $\delta^{13}C_{Cliff}$ ranges from -4.0 ‰ to -8.6 ‰, both consistent with isotopic values of CC3 stalagmite[51] (Fig. 2j). $\delta^{18}O_{Cliff}$ and $\delta^{13}C_{Cliff}$ do not show correlation, suggesting limited isotopic fractionation (Supplementary Table). We performed four Hendy tests to further attest that Cliff Cave stalagmite formed under isotopic equilibrium. Although the Hendy test is not always reliable due to variation in along-lamina's thickness[29], no major along-lamina $\delta^{18}O$ and $\delta^{13}C$ change was detected.

$\delta^{13}C_{Cliff}$ declines progressively towards lighter values until 9.0 ka, increases slightly up until 8.6 ka and then remains stable (Fig. SD4). This profile is very similar to that of $\delta^{13}C_{calcite}$ of Lake Inchiquin[34] (located ~20 km east from Cliff Cave; Fig. SD1). Diefendorf et al.[34] (and reference therein) attributed this $\delta^{13}C_{calcite}$ decline to a

lesser contribution of the surface weathered limestone bedrock to the lake due to the expansion of shrubs and trees in the region. On the basis of this interpretation, we interpret the millennial $\delta^{13}C_{Cliff}$ decline as a response to a vegetation expansion, which would prevent bedrock erosion and thereby result in lower $\delta^{13}C_{Cliff}$.

X-Ray Fluorescence (XRF) core scanning analysis

XRF analysis was performed using a Cox Analytical Itrax equipped with a molybdenum tube at the Department of Geological Sciences, Stockholm University. The instrument was operated with a step size of 200 µm and an exposure time of 40 s following Scroxton et al.[52]. The stalagmite surface was maintained horizontal and the XRF beam covered the central section (growth axis) of the stalagmite. Poor-quality data points were excluded if they did not fulfil the following criteria: validity =1, Ca counts > 1.7 E+6, mean squared error (MSE) >11, and a number of counts per second (CPS) > 82000. Each XRF data point is associated with a distance, starting when the core scanner detects x-rays. During our analysis, the Itrax detected x-rays slightly before the smooth surface of the stalagmite. We therefore adjusted the distance of the XRF data point. To do so, we used the position of drilling spots (corresponding to e.g., U-Th data) that were performed before the XRF scanning and which resulted in reduced XRF signals (Supplementary Table).

Cliff Cave stalagmite Sr/Ca data varies from 0.004 to 0.01 (Fig. 2e). When compared to existing Sr/Ca data obtained on speleothems with a similar Itrax instrument[52], the range of Cliff Cave stalagmite Sr/Ca values is relatively small, and suggests calcite as the dominant carbonate phase (Scroxton et al.,[52] reported a one-fold increase in Sr/Ca between calcite and aragonite). This is in good agreement with FTIR-ATR and XRD data. This also indicates that prior calcite precipitation (PCP) is limited; significant shift in Sr/Ca values would be expected otherwise. PCP (and degassing) affects stalagmite Sr/Ca ratio by shifting it to higher values[53]. The only observed increase in Sr/Ca_{Cliff} occurs between 11.1 and 8.6 ka (Fig. 2e). During this period, the growth rate of the stalagmite and its $\delta^{13}C$ do not co-vary with Sr/Ca ratio (Supplementary Table), indicating limited PCP. As mentioned in the previous section, it is possible that the establishment of trees and shrubs at the vicinity of the cave increased water infiltration (as opposed to runoff), thereby increasing the water residence time in the karst system resulting in the millennial-long Sr/Ca increase.

The decrease in Sr/Ca at 8.6 ka, coincides with (i) darker lamina, suggesting that more soil-derived organic material is transported into the cave, and (ii) to a period of relatively constant growth rate and $\delta^{13}C$ (Supplementary Table). Taken together, the Sr/Ca_{Cliff} decrease is coherent with a shift towards wetter soil conditions, while cave microclimate and its carbon sources remained relatively unchanged.

One-point-correlation map

We used the ERA5[41] dataset, which provides a reanalysis of climate variables based on a combination of climate model and observation data from 1950 to 2022, to calculate the one-point-correlation-maps of decadal mean temperatures at the cave location (coordinate: 53°N, 9°W).

References

1. Yang, Q. *et al.* Recent increases in Arctic freshwater flux affects Labrador Sea convection and Atlantic overturning circulation. *Nat. Commun.* **7**, (2016).

2. Madan, G., Gjermundsen, A., Iversen, S. C. & LaCasce, J. H. The weakening AMOC under extreme climate change. *Clim. Dyn.* **62**, 1291–1309 (2024).

3. Swingedouw, D. *et al.* Decadal fingerprints of freshwater discharge around Greenland in a multi-model ensemble. *Clim. Dyn.* **41**, 695–720 (2013).

4. Jackson, L. C. *et al.* Global and European climate impacts of a slowdown of the AMOC in a high resolution GCM. *Clim. Dyn.* **45**, 3299–3316 (2015).

5. Bellomo, K. *et al.* Impacts of a weakened AMOC on precipitation over the Euro-Atlantic region in the EC-Earth3 climate model. *Clim. Dyn.* **61**, 3397–3416 (2023).

6. Jackson, L. C. & Wood, R. A. Timescales of AMOC decline in response to fresh water forcing. *Clim. Dyn.* **51**, 1333–1350 (2018).

7. Martin, T., Biastoch, A., Lohmann, G., Mikolajewicz, U. & Wang, X. On Timescales and Reversibility of the Ocean's Response to Enhanced Greenland Ice Sheet Melting in Comprehensive Climate Models. *Geophys. Res. Lett.* **49**, (2022).

8. Robson, J., Hodson, D., Hawkins, E. & Sutton, R. Atlantic overturning in decline? *Nat. Geosci.* **7**, 2–3 (2014).

9. Rahmstorf, S. *et al.* Exceptional twentieth-century slowdown in Atlantic Ocean overturning circulation. *Nat. Clim. Chang.* **5**, 475–480 (2015).

10. Lochte, A. A. *et al.* Labrador Sea freshening at 8.5 ka BP caused by Hudson Bay Ice Saddle collapse. *Nat. Commun.* **10**, (2019).

11. Matero, I. S. O., Gregoire, L. J., Ivanovic, R. F., Tindall, J. C. & Haywood, A. M. The 8.2 ka cooling event caused by Laurentide ice saddle collapse. *Earth Planet. Sci. Lett.* **473**, 205–214 (2017).

12. Matero, I. S. O., Gregoire, L. J. & Ivanovic, R. F. Simulating the Early Holocene demise of the Laurentide Ice Sheet with BISICLES (public trunk revision 3298). *Geosci. Model Dev.* **13**, 4555–4577 (2020).

13. Dansgaard, W. *et al.* Evidence for general instability of past climate from a 250-kyr ice-core record. *Nature* **364**, 218–220 (1993).

14. Rohling, E. J. & Pälike, H. Centennial-scale climate cooling with a sudden cold event around 8,200 years ago. *Nature* **434**, 975–979 (2005).

15. Thomas, E. R. *et al.* The 8.2 ka event from Greenland ice cores. *Quat. Sci. Rev.* **26**, 70–81 (2007).

16. Gkinis, V. *et al.* A 120,000-year long climate record from a NW-Greenland deep ice core at ultra-high resolution. *Sci. Data* **8**, (2021).

17. Parker, S. E. & Harrison, S. P. The timing, duration and magnitude of the 8.2 ka event in global speleothem records. *Sci. Rep.* **12**, (2022).

18. Weaver, A. J., Sarachik, E. S. & Marotze, J. Freshwater flux forcing of decadal and interdecadal oceanic variability. *Nature* **353**, 836–838 (1991).

19. Vellinga, M. & Wood, R. A. Global Climatic Impacts of a Collapse of the Atlantic Thermohaline Circulation. *Clim. Change* **54**, 251–267 (2002).

20. Clark, P. U. *et al.* Freshwater Forcing of Abrupt Climate Change During the Last Glaciation. *Science (1979).* **293**, 283–287 (2001).

21. Gauthier, M. S., Kelley, S. E. & Hodder, T. J. Lake Agassiz drainage bracketed Holocene Hudson Bay Ice Saddle collapse. *Earth Planet. Sci. Lett.* **544**, (2020).

22. Barber, D. C. *et al.* Forcing of the cold event of 8,200 years ago by catastrophic drainage of Laurentide lakes. *Nature* **400**, 344–348 (1999).

23. Thornalley, D. J. R., Elderfield, H. & McCave, I. N. Holocene oscillations in temperature and salinity of the surface subpolar North Atlantic. *Nature* **457**, 711–714 (2009).

24. Ellison, C. R. W., Chapman, M. R. & Hall, I. R. Surface and deep ocean interactions during the cold climate event 8200 years ago. *Science (1979).* **312**, 1929–1932 (2006).

25. Hede, M. U. *et al.* Multiproxy evidence for terrestrial and aquatic ecosystem responses during the 8.2ka cold event as recorded at Højby Sø, Denmark. *Quat. Res.* **73**, 485–496 (2010).

26. Goslin, J. *et al.* Holocene centennial to millennial shifts in North-Atlantic storminess and ocean dynamics. *Sci. Rep.* **8**, (2018).

27. Stoll, H. M. *et al.* Rapid northern hemisphere ice sheet melting during the penultimate deglaciation. *Nat. Commun.* **13**, (2022).

28. Held, F. *et al.* Dansgaard-Oeschger cycles of the penultimate and last glacial period recorded in stalagmites from Türkiye. *Nat. Commun.* **15**, 1183 (2024).

29. McDermott, F. Palaeo-climate reconstruction from stable isotope variations in speleothems: A review. in *Quaternary Science Reviews* vol. 23 901–918 (2004).

30. Fairchild, I. J. *et al.* Modification and preservation of environmental signals in speleothems. *Earth. Sci. Rev.* **75**, 105–153 (2006).

31. Mullan, G. *et al. Caves of Mid-West Ireland*. (University of Bristol Speleological Society, 2019).

32. O'Connell, M. & Molloy, K. Mid- and late-Holocene environmental change in western ireland: New evidence from coastal peats and fossil timbers with particular reference to relative sea-level change. *Holocene* **27**, 1825–1845 (2017).

33. Lynch, M. The later Mesolithic on the North-West coast of Ireland. *Archaeology Ireland* **31**, 24–29 (2017).

34. Diefendorf, A. F., Patterson, W. P., Holmden, C. & Mullins, H. T. Carbon isotopes of marl and lake sediment organic matter reflect terrestrial landscape change during the late Glacial and early Holocene (16,800 to 5,540 cal yr B.P.): A multiproxy study of lacustrine sediments at Lough Inchiquin, western Ireland. *J. Paleolimnol.* **39**, 101–115 (2008).

35. Dominguez-Villar, D. *et al.* Oxygen isotope precipitation anomaly in the North Atlantic region during the 8.2 ka event. *Geology* **37**, 1095–1098 (2009).

36. Kim, S.-T. & O'Neil, J. R. Equilibrium and nonequilibrium oxygen isotope effects in synthetic carbonates. *Geochim. Cosmochim. Acta* **61**, 3461–3475 (1997).

37. Vacca, A. V., Bellomo, K., Fabiano, F. & von Hardenberg, J. On the role of AMOC weakening in shaping wintertime Euro-Atlantic atmospheric circulation. *Clim. Dyn.* **63**, (2025).

38. Smith, A. C. *et al.* North Atlantic forcing of moisture delivery to Europe throughout the Holocene. *Sci. Rep.* **6**, (2016).

39. Baldini, L. M., McDermott, F., Foley, A. M. & Baldini, J. U. L. Spatial variability in the European winter precipitation δ^{18}O-NAO relationship: Implications for reconstructing NAO-mode climate variability in the Holocene. *Geophys. Res. Lett.* **35**, (2008).

40. Morrill, C. *et al.* Proxy benchmarks for intercomparison of 8.2 ka simulations. *Climate of the Past* **9**, 423–432 (2013).

41. Hersbach, H. *et al.* The ERA5 global reanalysis. *Quarterly Journal of the Royal Meteorological Society* **146**, 1999–2049 (2020).

42. Reintges, A., Martin, T., Latif, M. & Keenlyside, N. S. Uncertainty in twenty-first century projections of the Atlantic Meridional Overturning Circulation in CMIP3 and CMIP5 models. *Clim. Dyn.* **49**, 1495–1511 (2017).

43. Ryan, C., Curley, M., Walsh, S. & Murphy, C. Long-term trends in extreme precipitation indices in Ireland. *International Journal of Climatology* **42**, 4040–4061 (2022).

44. Scholz, D. & Hoffmann, D. L. StalAge - An algorithm designed for construction of speleothem age models. *Quat. Geochronol.* **6**, 369–382 (2011).

45. Fankhauser, A., McDermott, F. & Fleitmann, D. Episodic speleothem deposition tracks the terrestrial impact of millennial-scale last glacial climate variability in SW Ireland. *Quat. Sci. Rev.* **152**, 104–117 (2016).

46. Stirling, C. H., Halliday, A. N. & Porcelli, D. In search of live 247Cm in the early solar system. *Geochim. Cosmochim. Acta* **69**, 1059–1071 (2005).

47. Andersson, P. S. & Schöberg, H. Determination of ^{232}Th and ^{230}Th in seawater using a chemical separation procedure and thermal ionization mass spectrometry. *Limnol. Oceanogr. Methods* **10**, 296–303 (2012).

48. Ludwig, K. R. User's Manual for Isoplot Version 3.75–4.15: a Geochronological Toolkit for Microsoft Excel. *Berkeley Geochronological Center Special Publication* **5**, (2012).

49. Richards, D. A. & Dorale, J. A. Uranium-series Chronology and Environmental Applications of Speleothems. *Rev. Mineral. Geochem.* **52**, 407–460 (2003).

50. Stracke, A., Scherer, E. E. & Reynolds, B. C. Application of Isotope Dilution in Geochemistry. in *Treatise on Geochemistry* 71–86 (Elsevier, 2014). doi:10.1016/B978-0-08-095975-7.01404-2.

51. Mcdermott, F. *et al. Holocene Climate Variability in Europe: Evidence from O, Textural and Extension-Rate Variations in Three Speleothems*. *Quaternary Science Reviews* vol. 18 (1999).

52. Scroxton, N. *et al.* Rapid measurement of strontium in speleothems using core-scanning micro X-ray fluorescence. *Chem. Geol.* **487**, 12–22 (2018).

53. Fairchild, I. J. *et al.* Controls on trace element (Sr–Mg) compositions of carbonate cave waters: implications for speleothem climatic records. *Chem. Geol.* **166**, 255–269 (2000).

54. McDermott, F., Mattey, D. P. & Hawkesworth, C. Centennial-Scale Holocene Climate Variability Revealed by a High-Resolution Speleothem 18 O Record from SW Ireland. *Science (1979).* **301**, 371 (2001).

55. Lewis, C. F. M., Miller, A. A. L., Levac, E., Piper, D. J. W. & Sonnichsen, G. V. Lake Agassiz outburst age and routing by Labrador Current and the 8.2 cal ka cold event. *Quaternary International* **260**, 83–97 (2012).

Figure captions

Figure 1: Cliff Cave within the context of the North Atlantic Ocean currents. Cliff Cave is located on the west coast of Ireland by a green star. Marine sediment cores mentioned in the text are shown in red circles. NAC: North Atlantic Current. NADW: North Atlantic Deep Water. ISOW: Iceland-Scotland Overflow Water. DSOW: Denmark Overflow Water. SPG: subpolar gyre. STG: subtropical gyre. Purple-shadowed area: approximate extent of the Laurentide ice sheet from Lochte et al.[10]. The Hudson Bay Ice Saddle (HBIS) is represented by the dashed area. Background geographic map: ESRI WorldMap (EPSG:4326 - WGS84).

Figure 2: Cliff Cave stalagmite $\delta^{18}O$ and Sr/Ca data compared to marine and terrestrial archives. a Cliff Cave stalagmite $\delta^{18}O$ timeseries. **b** Difference in $\delta^{18}O$ from planktonic and benthic foraminifera from marine sediment core RAPiD-12-1K[23]. **c** Salinity measurement of the sub-thermocline from RAPiD-12-1K[23]. **d** Grain size records – a proxy for the Iceland-Scotland Overflow Water strength – from marine sediment core MD99-2251[24]. **e** Cliff Cave stalagmite Sr/Ca timeseries. **f** $\delta^{18}O_c$ of *I. helena* (‰) identifying the onset of the freshwater signal of the HBIS collapse (dashed blue band)[10]. **g** Bottom Water Temperature reconstruction from MSM45-

19-2 identifying pre-HBIS collapse sub-surface warming in the Labrador Shelf[10]. **h** Abundance of *N. pachyderma* sinistra (s) from marine sediment core MD99-2251[24]. **i** Kaite Cave (KC; Spain) $\delta^{18}O$ timeseries recording two freshening episodes of the North Atlantic[35]. **j** Crag cave CC3 (Ireland) stalagmite $\delta^{18}O$ timeseries smoothed over a 5-average period[54] (anomalous data related to laser pencil technique have been removed accordingly to Fairchild et al.[30]). The light blue band brackets the timespan of the '8.2 ka' cooling anomaly as dated in speleothem records across the northern hemisphere[17]. Agassiz-Ojibway outburst revised ages from Lewis et al.[55]. Grey circles at the bottom of the figure: Cliff Cave stalagmite U-Th ages (2SD). GR: Growth rate profile of Cliff Cave stalagmite calculated at a 100-year interval using the ages modelled by StalAge. b2k: before year 2000 (all literature data are scaled to the b2k timescale).

Figure 3 Correlation between modern near surface temperature over Ireland and the North Atlantic storm track. **a** One-point correlation map of near-surface temperature from ERA5 reanalysis (1950-2022)[41] with current climate context. Note the delineation of the current North Atlantic warming hole[9]. **b** Same as (a) but the current climate context has been removed. Note the different scale bar between a and b. The band of highest correlation on both maps (in red) follows a NE-SW oriented pattern resembling the North Atlantic storm track as simulated in Jackson et al [4].

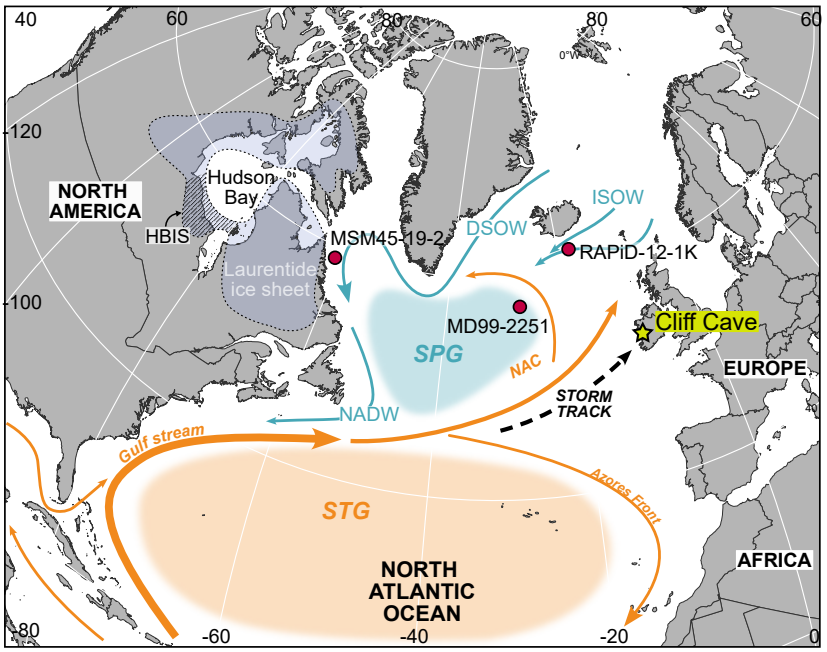
40
60
80
80
60
120
100
NORTH AMERICA
Hudson Bay
HBIS
Laurentide ice sheet
MSM45-19-2
ISOW
DSOW
RAPiD-12-1K
MD99-2251
SPG
NAC
Cliff Cave
EUROPE
STORM TRACK
NADW
Gulf stream
Azores Front
STG
NORTH ATLANTIC OCEAN
AFRICA
80
-60
-40
-20
0

Figure 1

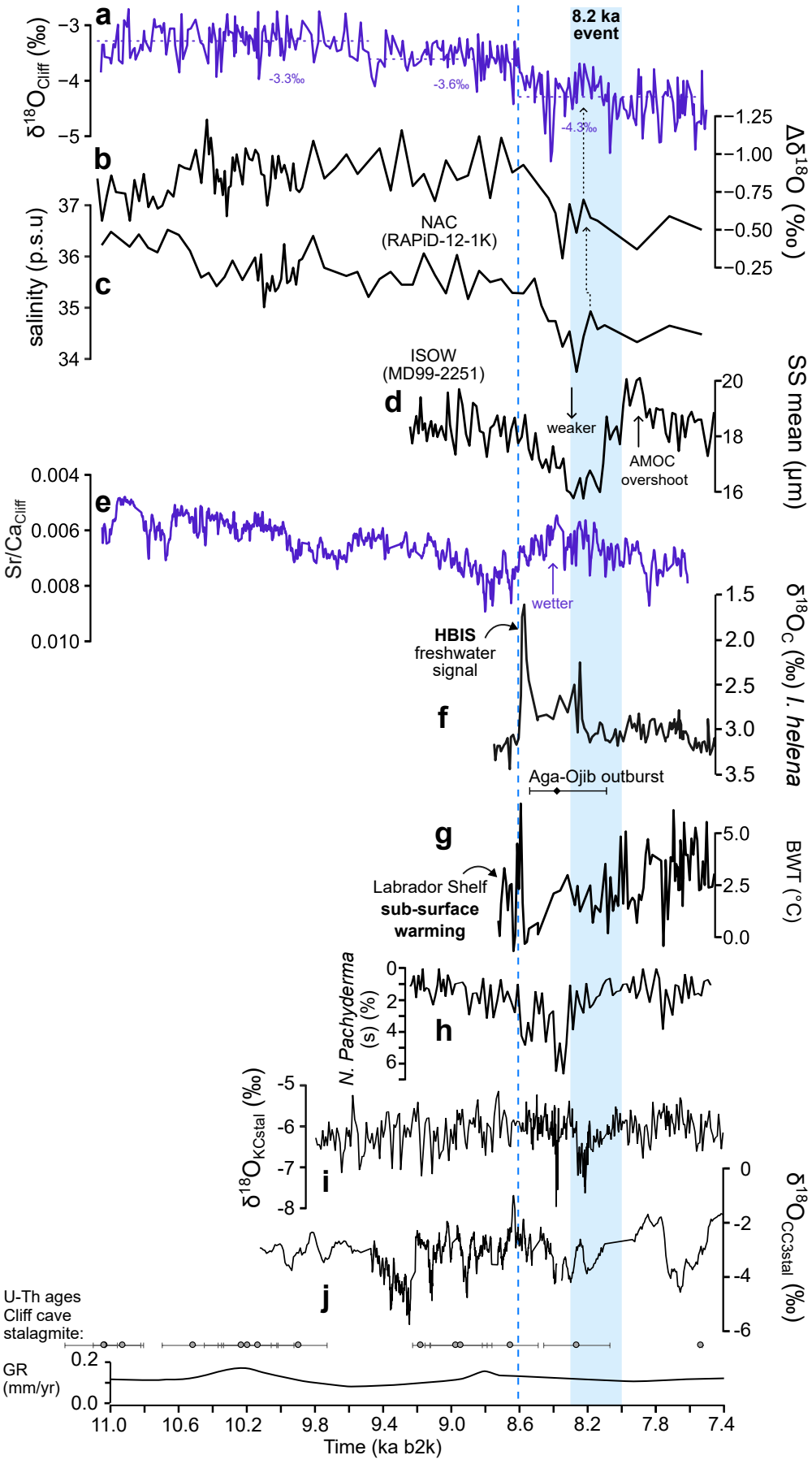
a
8.2 ka event
-3.3‰
-3.6‰
-4.3‰
δ18OCliff (‰)
b
NAC (RAPiD-12-1K)
Δδ18O (‰)
salinity (p.s.u)
c
ISOW (MD99-2251)
d
weaker
AMOC overshoot
SS mean (μm)
Sr/CaCliff
e
wetter
HBIS freshwater signal
f
δ18OC (‰) I. helena
Aga-Ojib outburst
g
Labrador Shelf sub-surface warming
BWT (°C)
N. Pachyderma (s) (%)
h
δ18OKCstal (‰)
i
j
δ18OCC3stal (‰)
U-Th ages Cliff cave stalagmite:
GR (mm/yr)
Time (ka b2k)

Figure 2

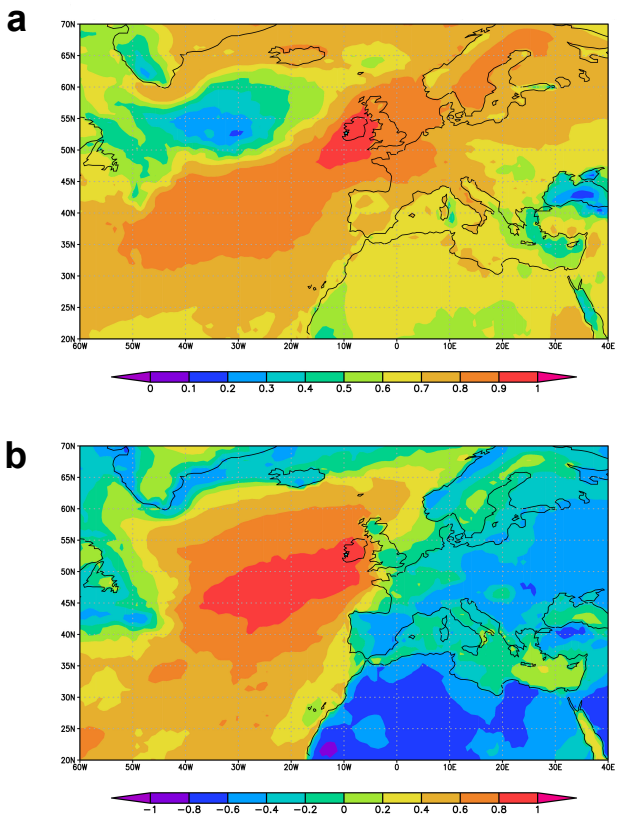
a
70N
65N
60N
55N
50N
45N
40N
35N
30N
25N
20N
60W
50W
40W
30W
20W
10W
0
10E
20E
30E
40E
0
0.1
0.2
0.3
0.4
0.5
0.6
0.7
0.8
0.9
1
b
70N
65N
60N
55N
50N
45N
40N
35N
30N
25N
20N
60W
50W
40W
30W
20W
10W
0
10E
20E
30E
40E
−1
−0.8
−0.6
−0.4
−0.2
0
0.2
0.4
0.6
0.8
1

Figure 3